Astron. Astrophys. 316, 449–456 (1996)

ASTRONOMY
AND
ASTROPHYSICS

Coronal radio sounding with Ulysses: dual-frequency phase scintillation spectra in coronal holes and streamers

M. Pätzold[1], **J. Karl**[1], **and M.K. Bird**[2]

[1] Institut für Geophysik und Meteorologie, Universität zu Köln, Albertus-Magnus-Platz, D-50923 Köln, Germany
[2] Radioastronomisches Institut, Universität Bonn, Auf dem Hügel 71, D-53121 Bonn, Germany

Received 18 March 1996 / Accepted 20 August 1996

Abstract. Dual-frequency Doppler measurements of the Ulysses downlink carrier signals were recorded during the spacecraft's 1995 solar conjunction. In this paper we present power spectra derived from phase fluctuations of the radio signals passing through the corona for different solar latitudes. It is possible to (a) distinguish clearly between spectra for which the ray paths were entirely embedded in a coronal hole or traversed a coronal streamer for the same solar offset distance of 25 solar radii and (b) characterize the evolution of the slope of the phase fluctuation spectra $p - 1$ as a function of heliolatitude, where p is the spectral index of the three-dimensional wavenumber spectrum of the electron density fluctuations. There is an obvious increase from p = 3.2 at high southern latitudes (coronal hole) toward the Kolmogorov value of $p = 11/3$ at those heliolatitudes coinciding with the extension of the heliospheric current sheet. The spectra show a local flattening with break frequencies at 0.06 Hz and 0.2 Hz for the hole and the streamer spectra, respectively. The shift from 0.06 Hz to 0.2 Hz is not gradual, but rather abrupt when the ray path becomes embedded in the streamer. The derived electron density fluctuations and fractional electron density fluctuations at 25 solar radii are larger in the coronal streamer than in the coronal hole by factors of ∼20 and ∼5, respectively.

Key words: Sun: corona – solar wind – occultation

1. Introduction

Observations of natural or spacecraft radio signals during solar occultations can provide important insights in the study of the solar corona over a wide range of distances including regions which can presently not be investigated *in situ*. Angular broadening and intensity scintillations have been used to study the fluctuations of electron density and the solar wind velocity as a function of heliocentric distance using galactic/extragalactic radio sources ("Interplanetary Scintillations": IPS; Kojima & Kakinuma 1987; Rickett & Coles 1991) or spacecraft radio signals. Phase scintillations of coherent monochromatic spacecraft radio signals are sensitive to a combination of electron density and solar wind velocity fluctuations (Woo 1975).

The Ulysses Solar Corona Experiment (SCE) sounded the solar corona during the spacecraft's superior solar conjunctions in summer 1991 and early 1995 using two coherent downlink frequencies at S-band (2.3 GHz) and X-band (8.4 GHz). The scientific objectives of SCE are the determination of the electron density profile as a function of heliocentric distance and latitude, measurements of solar wind velocity in its acceleration regime and investigation of coronal plasma turbulence (Bird et al. 1992). Results on the electron density distribution in the solar corona were published in Bird et al. (1994), Pätzold et al. (1995) and Bird et al. (1996, this issue). First estimates of the solar wind acceleration in coronal holes and streamers can be found in Pätzold et al. (1996). In this paper we present power spectra derived from phase fluctuations observed in coronal holes and streamers during the 1995 solar conjunction. Analysis of the phase fluctuations during the 1991 conjunction will follow in a subsequent paper.

2. Ulysses solar conjunctions

Fig. 1 presents the geometry of the Ulysses solar conjunction in early 1995, as viewed from Earth in the plane of the sky. The first Ulysses conjunction (C_1) occurred during the in-ecliptic phase of the mission on 21 August 1991. At this time the Ulysses ray path moved roughly radially from east limb to west limb, passing over the North pole of the Sun at an apparent solar offset distance (proximate solar point of the radio ray path) of R = 4.3 $R_\odot$ (solar radii). Contrasting with the common conjunction geometry of 1991, the apparent position of the spacecraft cut through the southwest quadrant of the solar corona from the South Pole to the solar equator in February-March 1995. This unique constellation was a consequence of the spacecraft's high inclination to the ecliptic plane. Radio-sounding observations were conducted

Send offprint requests to: Martin Pätzold

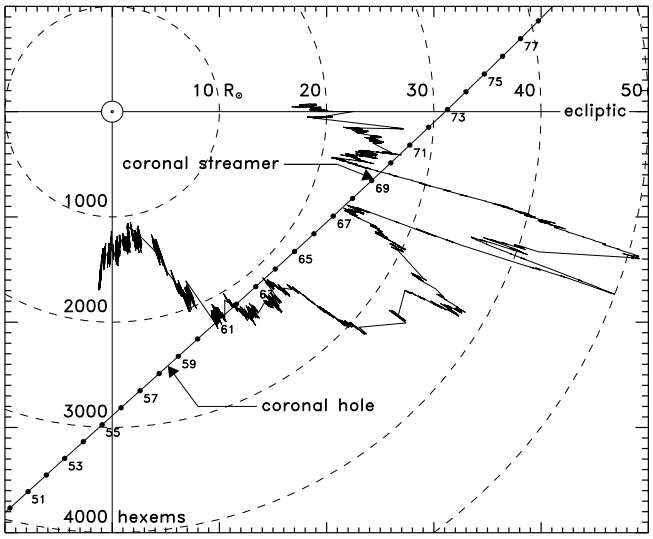

Fig. 1. Ulysses conjunction geometry in 1995. The dots indicate the apparent position of the spacecraft with respect to the Sun at 0 UT for each 1995 day-of-year (DOY) during the conjunction. Also included are measurements of the total electron content as a polar plot with the radial scale given along the south polar axis in units of hexems (10^{16} electron m^{-2}). Data recorded on DOY 58 and DOY 69, when the ... path was embedded in a coronal hole and a coronal streamer, ... discussed in this paper.

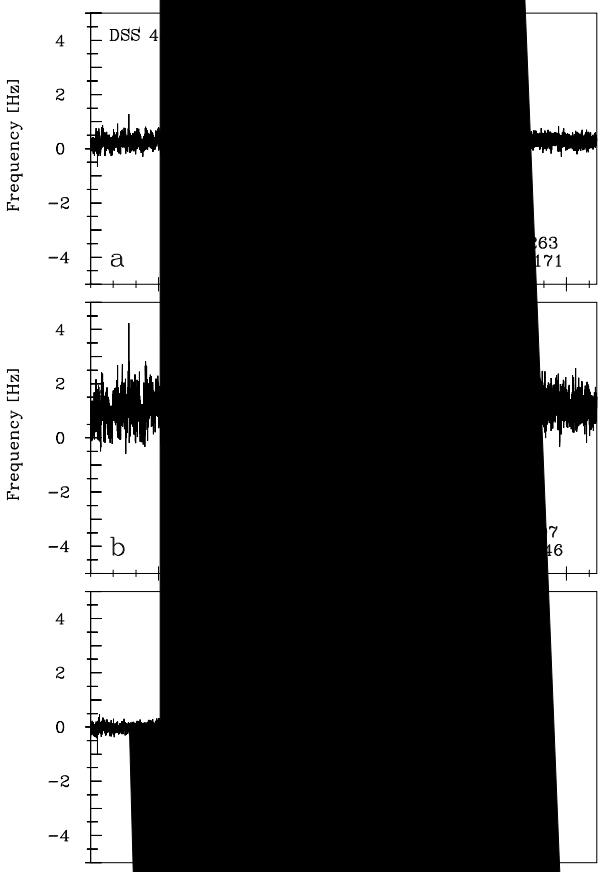

... proximately con-

... d X
... aft s
... in th
... way
... d upl
... ls w
... pple
... al Do
... whi
... ntent
... 0.31
c
... he spe
$= \int_0^s \delta$

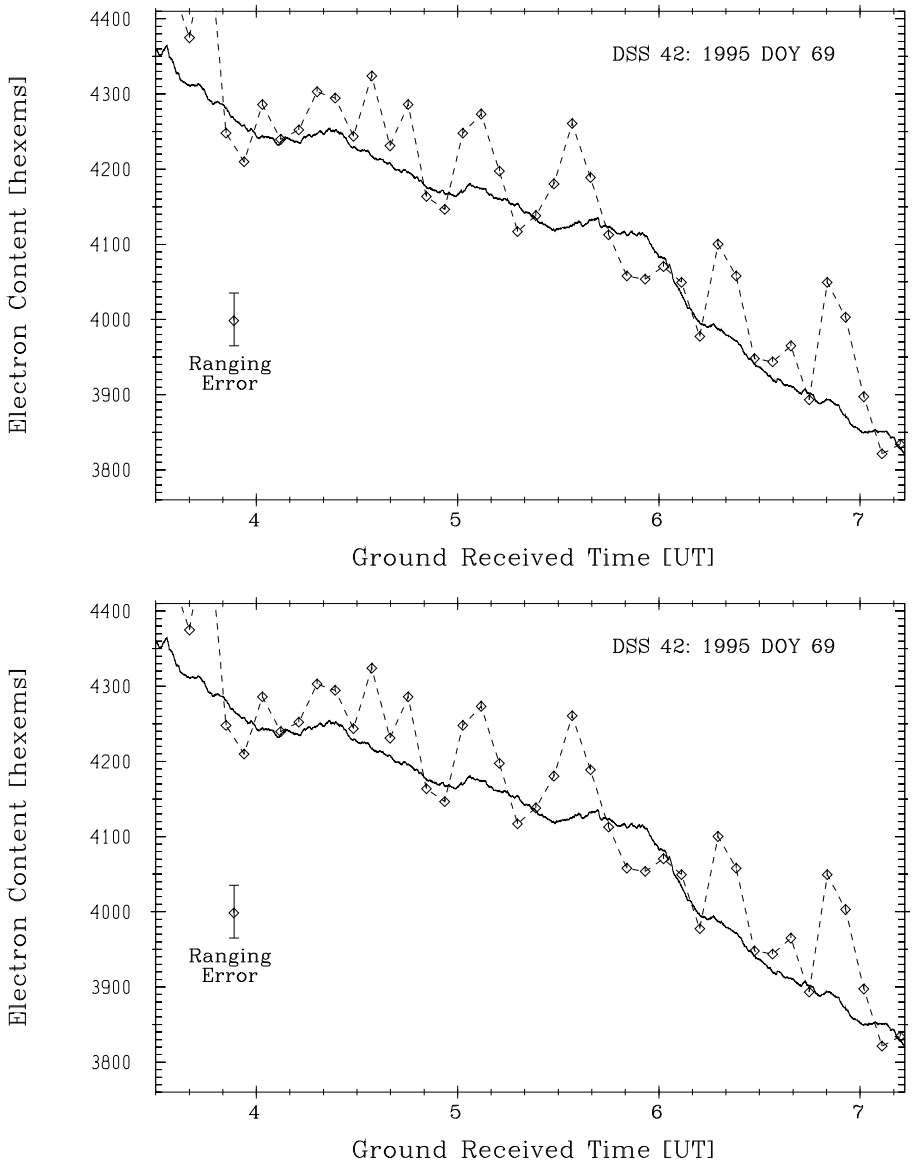

Fig. 3. a Differential phase, expressed in hexems, showing the change in electron content for the same tracking pass as shown in Fig. 2a–c. This is normalized to the total electron content as determined from the dual-frequency ranging data, shown as diamonds (Bird et al. 1996). **b** Differential phase residuals with subtracted baseline and trend in radians.

edge of a coronal hole (Pätzold et al. 1995). The ranging and Doppler data are in good qualitative agreement. The typical accuracy of the ranging points is ± 50 hexems while that of the differential Doppler measurement is of the order of ± 0.1 hexem (Bird et al. 1992). Subtracting the trend from the Doppler data in Fig. 3a yields the profile shown in Fig. 3b, now presented as differential phase in *radians*.

The power spectra were actually computed in the following manner. First the differential phase data are prewhitened by computing

$$\delta f_{i+1} = \frac{\Phi_{i+1} - \Phi_i}{t_{i+1} - t_i} \tag{5}$$

The differential Doppler data from Eq. (5), shown in Fig. 2a–cc, were spectral analysed using a standard FFT routine including a Parzen window and a block length of 4096 samples. The data interval represented in each spectrum is thus 4096 seconds and the spectral range extends from the lowest frequency at $2.4 \cdot 10^{-4}$ Hz to the Nyquist frequency at 0.5 Hz. The phase power spectrum is then obtained by dividing the frequency power spectrum by ν^2. The phase power spectrum calculated from the data of Figs. 2-3 is shown in Fig. 3 together with an a spectrum calculated from Doppler data obtained when Ulysses was at solar opposition (DOY 60, 1992). At solar opposition the contributions from the interplanetary medium are minimized and this spectrum represents a kind of calibration spectrum. Armstrong et al. (1979) observed Viking radio wave phase scintillation at various elongation angles ranging from 1° (solar conjunction) to 175° (solar opposition). The opposition spectrum shown in Fig. 3 is similar to the spectra published by Armstrong et al. (1979). The spectral power as a function of elongation decreases rapidly and approaches the level of a white noise spectrum for frequencies $\nu > 10^{-2}$ Hz.

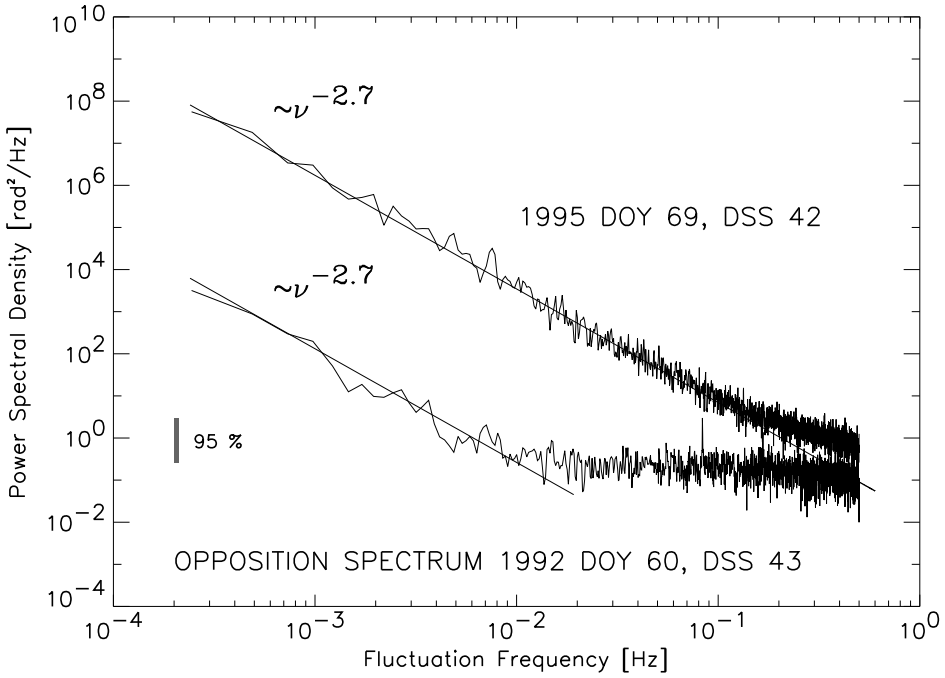

Fig. 4. Power spectrum (upper curve) calculated from the differential phase fluctuations
shown in Fig. 3b. The straight solid line represents a single power law fit with slope -2.7 in the frequency range $10^{-3}\text{Hz} \leq \nu \leq 5 \cdot 10^{-2}\text{Hz}$. The lower curve is a spectrum calculated from Doppler data obtained when Ulysses was at solar opposition. The contribution from the interplanetary medium is minimized at solar opposition. The slope for frequencies $\nu < 10^{-2}$ Hz is also -2.7. The power of the opposition spectrum is a white noise spectrum for frequencies $\nu > 10^{-2}$ Hz. The vertical bar denotes the 95% confidence level.

The three-dimensional electron density spectrum ist often described as a single power law

$$\Phi_{Ne}(q) \sim q^{-p} \tag{6}$$

over the wavenumber range $2 \cdot 10^{-6}\ \text{km}^{-1} \leq q \leq 0.1\ \text{km}^{-1}$, where $q = 2\pi \cdot \nu/v$ is the wavenumber, ν is the fluctuation frequency and v is the solar wind speed. Employing the Rytov approximation, Woo (1975) and Woo et al. (1976a, 1976b) obtained the two-way differential phase fluctuation spectrum $W_{\Phi d}(\nu)$ which should follow a single power law

$$W_{\Phi d}(\nu) = (0.857)(0.033) c_{no}^2 \left[\frac{2\pi f_S}{c}\right]^2 \frac{8\pi^3 a_1 R}{v} \cdot \left[\frac{2\pi\nu}{v}\right]^{1-p} \frac{\Gamma((p-1)/2)}{\Gamma(p/2)} \tag{7}$$

with slope $1 - p$, where p is the spectral index of the three-dimensional wavenumber spectrum of electron density fluctuations, $a_1 = 0.85$ (Woo 1975), f_S is the S-band carrier frequency, R is the closest approach distance of the ray path to the Sun, c_{no} is the structure constant which indicates the strength of turbulence, v is the solar wind velocity transverse to the ray path at the proximate point to the Sun, ν is the fluctuation frequency and Γ is the Gamma Function.

The phase fluctuation spectrum shown in Fig. 3 represents a typical spectrum with slope $p - 1 \simeq 2.7$, indicating that the spectral index of the 3-D spatial spectrum of electron density inhomogenieties $p \simeq 3.7$. The dashed line is a single power law fit to the data in the frequency range 10^{-3} Hz $\leq \nu \leq 5 \cdot 10^{-2}$ Hz. Assuming a solar wind velocity of 350 km s^{-1}, this corresponds to a spatial wavenumber range of $1.8 \cdot 10^{-5}\ \text{km}^{-1} \leq q \leq 9 \cdot 10^{-4}\ \text{km}^{-1}$. Similar spectra have been derived from observational data of different spacecraft during solar conjunction (Mariner 10, Viking, Pioneer 10 and 11), reported by Woo et al. (1976a, 1976b), Woo & Armstrong (1979) and Tyler et al. (1981).

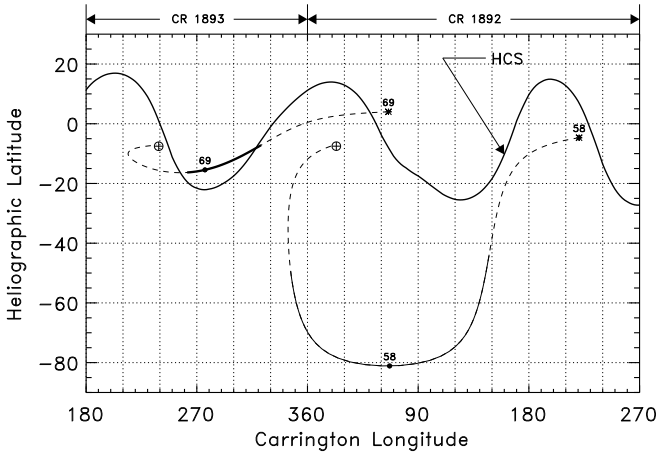

Fig. 5. Projections of the radio ray paths on DOY 58 and DOY 69 from Ulysses (position at star) to Earth (⊕) onto the Source Surface Map. The thick solid line marked HCS is the heliospheric current sheet as determined from observations at the Wilcox Solar Observatory (courtesy J.T. Hoeksema, Stanford University)

The Ulysses data from the 1995 conjunction enable one to (a) distinguish clearly between spectra for which the ray paths at the same solar offset distance were entirely embedded in a coronal hole or traversed a coronal streamer, and (b) characterize the evolution of the spectral index p as a function of heliolatitude.

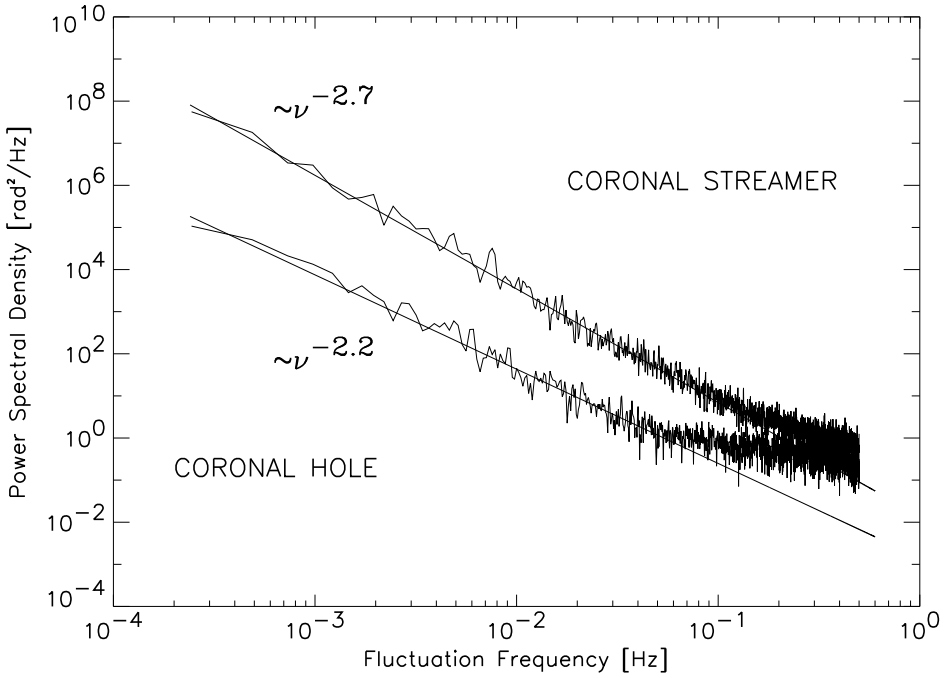

Fig. 6. Phase fluctuation spectra derived from observations on DOY 58 and DOY 69 when the radio ray paths passed mostly through a coronal hole and mostly through the heliospheric current sheet, respectively. It is evident that the spectral index $p-1$ is significantly smaller and that there is less power contained in the coronal hole spectrum. The two data sets were recorded at almost the same heliocentric solar offset distance of 25 $R_\odot$.

4. Ulysses phase spectra during the 1995 conjunction

As mentioned previously (Fig. 1) the Ulysses radio ray path sampled all heliographic latitudes at ca. 0.1 AU during the 1995 conjunction. It was determined (Pätzold et al. 1995) that the ray paths on the 1995 days of year (DOY) 54 to at least 64 were entirely embedded in the southern coronal hole. Examples of two ray path projections onto the source surface map of the radial coronal magnetic field are shown in Fig. 5. Whereas the projected ray path on DOY 58 was embedded within the south polar coronal hole, the ray path on DOY 69 ran basically parallel to and within the heliospheric currect sheet (HCS), the interplanetary extension of a coronal streamer (see also Fig. 1).

Fig. 3 shows a comparison of the two spectra, one obtained in the southern coronal hole on DOY 58 and the other in a streamer on DOY 69 at essentially the same heliocentric distance of 25 $R_\odot$, but different heliographic latitude. It is striking that the spectral index of the streamer sprectrum is steeper $(p-1)_{streamer}$ = 2.7 than that of the coronal hole $(p-1)_{hole}$ = 2.2. There is also a significant difference in the power level of the two spectra, which increases towards smaller ν.

Fig. 7 (upper panel) shows the spectral index $(p-1)$ over the range of fluctuation frequencies from 10^{-3} Hz $\leq \nu \leq 5 \cdot 10^{-2}$ Hz, computed for all tracking passes during the 1995 conjunction as a function of heliographic latitude. There is an obvious increase in $(p-1)$ toward the Kolmogorov value $(11/3-1)$ at those heliographic latitudes coinciding with the extension of the HCS.

Another striking feature of the spectra in Fig. 3 is their flattening above a break frequency at 0.2 Hz and 0.06 Hz for the streamer and the hole spectrum, respectively. The spectra of all Doppler tracking passes taken in the coronal hole and the spectra taken in the region of the HCS seem to flatten at these

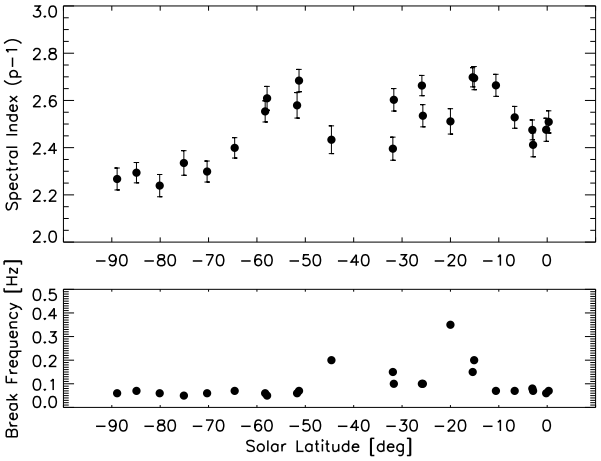

Fig. 7. Spectral parameters as a function of the heliographic latitude of the solar offset point. Upper panel: spectral index $p-1$; lower panel: spectral break frequency.

frequencies. There is no gradual increase from 0.06 Hz toward 0.2 Hz, but rather a more abrupt shift (Fig. 7 lower panel), in contrast to the more or less continuous transition in spectral index shown in Fig. 7 (upper panel). It seems that this behaviour is connected to the vicinity of the HCS and thus with the solar wind speed. The spectra do not flatten into a white spectrum as might be expected if running into a noise floor. The slope of the flattened part of the spectrum was determined to be -1.5 and -0.7 for the streamer and the hole, respectively. A similar flattening was not observed in the spectrum shown by Woo et al. (1976b) because the Nyquist frequency of the Mariner 10 spectra (0.05 Hz) was below the break frequency.

Woo and Armstrong (1979), in their analysis of the extensive Viking radio scattering data set, found that the spectral index varies with heliocentric distance, being less than $(11/3 - 1)$ for distances $R < 20$ $R_\odot$ and Kolmogorov for larger distances. The 1995 Ulysses spectral index data in Fig. 7 are in agreement with the Viking data for the coronal streamer at 25 $R_\odot$, but show distinctly smaller spectral indices for the coronal hole at 25 $R_\odot$. Woo and Armstrong (1979) did also not distinguish between holes and streamers and assumed a generally constant solar wind velocity.

Marsch and Tu (1990), in an extensive analysis of Helios plasma measurements in the distance range 0.3–1.0 AU, determined spectral indicies of electron density spectra for both slow and fast solar wind. They found a significant flattening for the fast solar wind in the frequency range $5 \cdot 10^{-4}$ Hz $\leq \nu \leq 2 \cdot 10^{-3}$ Hz, applicable to the Ulysses observations reported here. Their results imply a 3D spectral index of $p \simeq 3.5$ for slow wind ($v \simeq 300$ km s^{-1}) and p $\simeq 2.5$ for fast wind ($v \simeq 700$ km s^{-1}).

5. Discussion

Evidently, it is inadequate to describe the density spectrum by a pure power law as done by Armstrong and Woo (1979). Coles and Harmon (1989) found that the density spectrum near the Sun is well represented by a three-component model: (*i*) a Kolmogorov-like spectrum in the scale range $10^6 - 10^3$ km with wavenumbers $6.3 \cdot 10^{-6}$ km$^{-1} \leq q \leq 6.3 \cdot 10^{-3}$ km^{-1}, corresponding to the frequency range $2 \cdot 10^{-4}$ Hz $\leq \nu \leq 0.2$ Hz for the slow wind (v = 200 km s^{-1}) and $7 \cdot 10^{-4}$ Hz $\leq \nu \leq 0.7$ Hz for the fast wind (v = 700 km s^{-1}); (*ii*) a flattening at scales between 1000 km and the inner scale of $\approx$ 10-100 km, and (*iii*) a final steepened part at high frequencies, attributed to dissipation at scales near 10 km (20 Hz and 70 Hz for the slow and the fast wind, respectively).

Manoharan et al. (1994) found a dependence of the density spectrum on the solar wind speed at frequencies above 1 Hz. Steeper spectra were found for the higher velocities, i.e. exactly opposite to the trend found in the Ulysses data at lower frequencies. It is possible that the power at high frequencies is affected by dissipation near the inner scale, however, leading to an apparent steeper spectrum for the fast wind. Coles and Harmon (1989) found a Kolomogorov-like spectrum at frequencies below 10^{-4} Hz, a flattened region at frequencies $\approx 10^{-3} - 10^{-1}$ Hz, and a much steeper spectrum at higher frequencies.

The Ulysses data presented here are applicable to the frequency range $2.4 \cdot 10^{-4}$ Hz $\leq \nu \leq 0.5$ Hz or scales $7 \cdot 10^5$ km $\geq s \geq 400$ km for the slow wind and $2.6 \cdot 10^6$ km $\geq s \geq 1,400$ km for the fast wind. They were recorded at a solar distance intermediate to the range valid for the investigations of Coles and Harmon (1989) at 5–20 $R_\odot$ and Manoharan et al. (1994) at $R > 70$ $R_\odot$.

Measured and calculated physical quantities based on the spectra displayed in Fig. 3 are listed in Table 1.

Woo et al. (1976) have shown and Woo & Armstrong (1979) have used the fact that if the three-dimensional wavenumber spectrum Φ_{ne} of the electron density fluctuations has a power law dependence with spectral index p, then the one-dimensional frequency spectrum of electron density fluctuations V_{ne} has a power law dependence with spectral index $p - 2$. The spectrum V_{ne} is observed *in situ* by solar wind analysers on spacecraft. For $R < 100 R_\odot$, V_{ne} is related to $W_{\Phi d}$ (Woo & Armstrong 1979) by

$$V_{ne}(\nu) = 4.39 \cdot 10^{27} \cdot W_{\Phi d}(\nu) \frac{\nu}{v \cdot R} \left[\frac{2\pi f_S}{c}\right]^2 \frac{1}{p-2} \frac{\Gamma(\frac{p}{2})}{\Gamma(\frac{p-1}{2})} \quad (8)$$

The ratio of the power level at a given fluctuation frequency ν in a coronal streamer to that in a coronal hole is thus

$$\begin{aligned} \frac{V_{ne,streamer}(\nu)}{V_{ne,hole}(\nu)} &= \frac{W_{\Phi d,streamer}}{W_{\Phi d,hole}} \cdot \frac{v_{hole}}{v_{streamer}} \cdot \\ &\quad \frac{p_{hole} - 2}{p_{streamer} - 2} \cdot \\ &\quad \frac{\Gamma(\frac{p_{streamer}}{2})}{\Gamma(\frac{p_{streamer}-1}{2})} \cdot \frac{\Gamma(\frac{p_{hole}-1}{2})}{\Gamma(\frac{p_{hole}}{2})} \end{aligned} \quad (9)$$

It is assumed that the acceleration of the fast wind is already terminated at $25 R_\odot$ (Grall et al. 1995), so that v_{hole} = 700 km/s. Assuming further that the slow wind is still being accelerated inside 40 - 70 $R_\odot$ (Pätzold et al. 1996), a reasonable range of velocities is 100 km/s $\leq v_{streamer} \leq$ 350 km/s. Under these assumptions the ratio given by (9) lies in the range $2400 \geq V_{ne,streamer}/V_{ne,hole}(\nu_0 = 2.8 \cdot 10^{-4}$ Hz$) \geq 700$.

Woo et al. (1976b) derived an expression for the rms fluctuation of the electron density σ_{ne}, which, together with Eq. 7, may be written as

$$\begin{aligned} \sigma_{ne}(\nu_0) &= \left[0.033 \cdot c_{n0}^2 \cdot 2\pi \cdot L_0^{p-3} \frac{\Gamma(\frac{3}{2})\Gamma(\frac{p-3}{2})}{\Gamma(\frac{p}{2})}\right]^{\frac{1}{2}} \cdot \\ &\quad 5.66 \cdot 10^{13} \cdot \left[\frac{2\pi f_S}{c}\right]^2 \quad (10) \\ &= \left[\frac{W_{\Phi d}}{0.857} \cdot \frac{L_0^{p-3} \cdot v}{a_1 \cdot R} \cdot \left[\frac{2\pi\nu_0}{v}\right]^{p-1} \cdot \frac{\Gamma(\frac{3}{2})\Gamma(\frac{p-3}{2})}{\Gamma(\frac{p-1}{2})}\right]^{\frac{1}{2}} \cdot \\ &\quad 5.66 \cdot 10^{13} \cdot \frac{f_S}{c} \quad (11) \end{aligned}$$

where $L_0 = v/(2\pi \cdot \nu_0)$ is the maximum scale of turbulence at the selected minimum fluctuation frequency $\nu_0 = 2.8 \cdot 10^{-4}$ Hz corresponding to the averaging time interval. Using further the fact that

$$\begin{aligned} \Gamma\left(\frac{3}{2}\right) &= \frac{\sqrt{\pi}}{2} \\ \Gamma\left(\frac{p-3}{2}\right) &= \frac{2}{p-3}\Gamma\left(\frac{p-1}{2}\right) \end{aligned}$$

Table 1. Phase scintillations and derived quantities: coronal streamer vs. coronal hole

	coronal streamer	coronal hole
observed quantities:		
DOY	69	58
solar offset distance R [$R_\odot$]	25	25
heliolatitude of solar offset point [deg]	-79	-15
$W_{\Phi d}(\nu_0 = 2.8 \cdot 10^{-4})$ [rad^2/Hz]	$5{\cdot}10^7$	$1.2 \cdot 10^5$
$p-1$	2.7	2.2
break frequency [Hz]	0.2	0.06
calculated quantities at 25 $R_\odot$:		
$V_{ne}(\nu_0 = 2.8 \cdot 10^{-4}$Hz) [cm^{-6} Hz^{-1}]	$5.1 \cdot 10^7$...$1.4 \cdot 10^{7\ (a)}$	$2.1 \cdot 10^{4(b)}$
$\sigma_{ne}(R)$ [cm^{-3}]	243...130$^{(a)}$	7.6$^{(b)}$
$N_e(R)$[cm^{-3}]	950$^{(c)}$	200$^{(c)}$
$\sigma_{ne}(R)$ / $N_e(R)$[%]	25...13.5$^{(a)}$	3.8$^{(b)}$

$^{(a)}$ assumed slow solar wind velocity range at 25 $R_\odot$: 100–350 km s^{-1}
$^{(b)}$ assumed fast solar wind velocity at 25 $R_\odot$: 700 km s^{-1} (Phillips et al. 1995)
$^{(c)}$ estimates from measurements of column densities (Bird et al. (1996)

σ_{ne} reduces to the form

$$\sigma_{ne} = \left[\frac{W_{\Phi d}}{0.857} \cdot \frac{(2\pi)^2}{v \cdot a_1 \cdot R} \cdot \frac{\sqrt{\pi}}{p-3} \cdot \nu_0^2\right]^{\frac{1}{2}} \cdot 5.66 \cdot 10^{13} \cdot \left[\frac{f_S}{c}\right] \quad (12)$$

The ratio of the rms electron density fluctuation in a coronal streamer to a coronal hole, valid for averaging time intervals of ca. one hour ($\nu_0 = 2.8 \cdot 10^4$ Hz), is thus given by

$$\frac{\sigma_{ne,stream}}{\sigma_{ne,hole}} = \left[\frac{W_{\Phi d,stream}}{W_{\Phi d,hole}} \cdot \frac{v_{hole}}{v_{stream}} \cdot \frac{p_{hole}-3}{p_{stream}-3}\right]^{\frac{1}{2}} \quad (13)$$

Using the range of solar wind speeds mentioned in Table 1 for the fast and slow wind, the streamer-to-hole ratio from Eq. 13 found to be in the range $32 \geq \sigma_{ne,streamer}/\sigma_{ne,hole}(\nu_0) \geq 17$. Coles et al. (1995) found a deficiency of σ_{ne}^2 in the polar streams during the declining phase of the solar cycle in the order of 15 for wavenumbers in the order of 0.01km^{-1} or 0.3 Hz, corresponding to a ratio $\sigma_{ne,streamer}/\sigma_{ne,hole} \sim 3.8$. The values inferred in this work are valid for much smaller frequencies or wavenumbers and reflect the increasing divergence of the two spectra of the lower frequencies.

Values for $V_{ne}(\nu_0)$ and $\sigma_{ne}(\nu_0)$ derived from the hole and the streamer spectra can be found in the lower part of Table 1. $V_{ne}(\nu_0)$ is consistent with the electron density fluctuation spectra derived from the Viking data set (Woo & Armstrong 1979) for the given range of slow solar wind velocities.

The fractional density fluctuation $\sigma_{ne}(\nu_0)/N_e$ is listed in Table 1 for different slow solar wind velocities at R = 25 $R_\odot$ and for an already terminated solar wind acceleration in the fast solar wind stream (Grall et al. 1995) with an asymptotic velocity of 700 km s^{-1} (Phillips et al. 1995). The electron densities were taken from the model of Bird et al. (1996) based on Ulysses electron content measurements. The ratio of the fractional electron density variations in the streamer and the hole is thus in the range $5.3 \geq \sigma_{streamer} N_{hole}/\sigma_{hole} N_{streamer} \geq 3.5$. The derived fractional electron densities can be compared with Woo et al. (1995), who obtained ratios of 15% and <3% for streamer and hole, respectively, valid for fluctuations at periods up to 5 hours. In view of the divergence of the spectra coronal hole vs. coronal streamer at long periods, it is not surprising that Woo et al. (1995) derived a somewhat larger difference in the respective fractional density fluctuations.

Acknowledgements. We thank W.A. Coles for valuable comments and discussion. This experiment could not have been performed without the support of the Ulysses project office, the Deep Space Network and the Multi Mission Radio Science Support Team. It is a pleasure to thank N. Angold, S.W. Asmar, J. Caetta, D. Chong, P. Eshe, R. Garcia Pérez, R. Herrera, T. Horton, A. Knight, T.P. McElrath, D. Meyer, and T. Priest, all at the Jet Propulsion Laboratory. This work was supported by the Deutsche Agentur für Raumfahrtangelegenheiten (DARA) under grants 50 ON 9401 and 50 ON 9104. The responsibility for the contents of this publication is assumed by the authors.

References

Armstrong J.W., Woo, R., Estabrook F.B., 1979, ApJ 230, 570
Bird M.K., Asmar S.W., Brenkle J.P., Edenhofer P., Pätzold M., Volland H., 1992, A&AS 92, 425
Bird M.K., Volland H., Pätzold M., Edenhofer P., Asmar S.W., Brenkle J.P., 1994, ApJ 426, 373
Bird M.K., Pätzold M., Edenhofer P., Asmar S.W., McElrath T.P., 1996, A&A, this issue
Coles W.A., Harmon J.K., 1989, ApJ 337, 1023
Coles W.A., Grall R.R., Klinglesmith M.T., Bourgois G., 1995, J. Geophys. Res. 100, 17069
Grall R.R., Coles W.A., Klinglesmith M.T., Breen A.R., Williams P.J.S., Markkanen J., Esser R., 1995, Nature 379, 429
Kojima M., Kakinuma T., 1987, J. Geophys. Res. 92, 7269
Manoharan P.K., Kojima M., Misawa H., 1994, J. Geophys. Res. 99, 23,411
Marsch E., Tu C.-Y., 1990, J. Geophys. Res. 95, 11945

Pätzold M., Bird M.K., Edenhofer P., Asmar S.W., McElrath T.P., 1995, Geophys. Res. Lett. 22, 3313
Pätzold M., Tsurutani B.T., Bird M.K., 1996, *Solar Wind 8 Proceedings*, in press
Phillips J.L., Bame S.J., Barnes A., Barraclough B.L., Feldman W.C., Goldstein B.L., Gosling J.T., Hoogeveen G.W., McComas D.J., Neugebauer M., Suess S.T., 1995, Geophys. Res. Lett. 22, 3301
Rickett B.J., Coles W.A., 1991, J. Geophys. Res. 96, 1717
Tyler G.L., Vesecky J.F., Plume M.A., Howard H.T., Barnes A., 1981, ApJ 249, 318
Woo R., 1975, ApJ 201, 238
Woo R., Armstrong J.W., 1979, J. Geophys. Res. 84, 7288
Woo R., Yang F., Ishimaru A., 1976a, ApJ 210, 593
Woo R., Yang F., Yip K.W. Kendall W.B., 1976b, ApJ 210, 568
Woo R., Armstrong J.W., Bird M.K., Pätzold M., 1995, Geophys. Res. Lett. 22, 329